# NUMERICAL INVESTIGATION OF VPD PROCESS FOR DRYING OF TRANSFORMER'S INSULATION PAPER

***Cemil YIGIT[1,*], Ahmet AYDIN [2], Halit YASAR [1], Fatih ISIK[3], Tahsin ENGIN [1]***

[*1] Department of Mechanical Engineering, Sakarya University, Sakarya, Turkey

[2] Research and Development Center, Sakarya University, Sakarya, Turkey

[3] Astor Research and Development Center, Ankara, Turkey

[*] Corresponding author; E-mail: cyigit@sakarya.edu.tr

*The moisture content of oil-filled transformers insulation paper that is a cellulose-containing material comprises 8 to 10% of moisture by weight at ambient temperature and it is highly important to decrease the moisture content for effective use of a transformer. Vapor phase drying is more effective method for drying the insulation paper of the transformer as compared with other conventional methods due to less cycle time and energy consumption. The purpose of this paper is to design a solvent operated drying chamber in which drying of the insulation paper of oil filled transformer carried out. The approach of the present paper is to develop a numerical model to reduce the cycle time of the drying process. The unsteady flow, heat and mass transfer phenomena were simulated by using computational fluid dynamics solver. Theoretical studies and a numerical model were conducted over thermal calculation in the drying process using solvent at different pressures. Theoretical calculations were used to validate the numerical model. Drying chamber was optimized by using response surface methodology. The result of the study showed that drying cycle time was decreased almost 14.3% with the new design. Furthermore, when the solvent was used instead of air as a heat carrier, the drying cycle time was reduced.*

Key words*: Vapor Phase Drying, Transformers, Computational Fluid Dynamics.*

## 1. Introduction

Transformers have great importance for the transmission, distribution, and utilization of alternating current electrical energy. Laminated core, windings and insulating materials are primary parts of the transformers. Construction of transformers requires insulation that covers the windings. Insulating paper, due to its low cost and desirable physical and electrical properties, is used in oil filled transformer to isolate the primary and the secondary circuit from each other and from the transformer core. High temperatures, oxidation processes, and moisture are the primary enemies of the cellulose-based insulation system, which must have a moisture holding capacity of about 8-10% according to IEC standarts toprevent breakage during assembly. The ability of transformers to operate efficiently and for a longer period of time depends on reducing this moisture content. The mechanical life is

reduced by half for each doubling water content [1]. Drying process is extremely influential on the performance of the transformers. When the water content in oil of oil filled transformer that is the subject of this study increases from 10 ppm to 20 ppm, the impulse strength decreases by 20%. Furthermore, an increase in water content from 0.15% to 0.20%, reduces impulse strength by about 14% [2, 3].

Some methods, such as spray drying, vacuum drying, and air-drying have been reported in literature in order to improve the efficiency and activity of the drying process. For instance, Orikasa et al. [4] investigated the effect of hot air and vacuum drying methods in food industry (in drying process of kiwifruit slices). They found that quality features of the product by vacuum drying method were considerably lower than those by hot air drying method. Padmanabhan et al. [5] examined the vacuum drying method on silica cryogel-glass fiber blanket and obtained low density and thermal conductive silica cryogel-glass fiber blankets in their study. They claimed that vacuum drying method is relatively cost-effective, safe and timesaving method. Some researchers [6-8] used the spray drying method by optimizing the operating conditions with the response surface methodology to produce a powder of various foods. Others [9-12] used this method to produce some electrochemical materials. Additionally; there are researchers [13-19] who had examined the application of drying method in order to optimize the drying kinetics and uniformity. Although mentioned methods effectively used in food and electrochemical industry, due to temperature limitation, they are not capable of necessary dehumidification in power transformers. The insulation drying time increases with the size of the transformer and it is very difficult to obtain a uniform temperature distribution by spray drying in the long drying periods. Besides, long drying periods causes the higher partial discharge inception voltage.

Vapor phase drying (VPD) process in which a hydrocarbon solvent is used due to the difference in vapor pressure between water and solvent, is currently an effective drying method for the insulation and active parts of transformers. Since the solvent cleans the dust and dirt on the transformer, VPD process is to be done in a shorter time and at a lower temperature than vacuum drying (VD) process. This will reduce energy consumption. The energy consumption of the VD process on the low power transformer (> 3000 kVA) is about 17% less than the VPD process. Whereas the energy consumption of VPD process on the large power transformer is on about 6% less than the VD process. The cycle time of the VPD process is 20% to 30% shorter than the VD process, depending on the transformer power [3]. When compared with conventional methods, the VPD method leaves less residual moisture in the insulating paper after drying process. In addition, due to low partial vapor pressure and viscosity and high flash point of solvent moisture is reduced without damaging the insulation paper.

In order to improve this process even more a numerical study can be developed. Therefore, in this paper, a theoretical and numerical study over temperature distribution on the insulation paper in the VPD process using solvent at different pressures was conducted. The drying process was optimized using computational software to improve drying chamber design.

## 2. Drying process

### 2.1. Vapor phase drying

VPD is the method that has two heating phase, and the heating process of the method is conducted with the vapor of low viscosity solvent. The solvent vapor condenses in the drying chamber, and it is pulled out from drying chamber by the vacuum pump.

The drying process consists of preparation, heating and drying, pressure reduction and fine vacuum stages. In the preparation stage, the chamber pressure is reduced to the level of 6 mbar with full vacuum. The solvent is heated up to 403 K in the evaporator and solvent vapor enters into the vacuum chamber. In the heating and drying stage, the solvent vapor is condensed due to temperature and concentration differences. At the end of this phase, solvent vapor, water vapor, and air are formed in the drying chamber. This gas mixture is discharged using a vacuum pump for recirculation. In the pressure reduction stage, solvent vapor feed is stopped and solvent vapor condensed in the condenser and sent to the evaporator. The pressure reduction operation is terminated when the pressure in the drying chamber reaches 26 mbar. In the fine vacuum stage, pressure is reduced to the level of 1 mbar, and the solvent is drained from the vacuum chamber. When the residual moisture at the active parts of the transformer is less than 0.3%, the cycle is stopped [3, 20].

### 2.2. Properties of solvent and water

ShellSol D40 is used as the solvent in this study. It is a hydrogenated solvent that consists predominantly of C9- C11 paraffin and naphthenic. The vapor pressure of ShellSol D40 and water is 0.08 kPa and 2.66 kPa at the temperature of 293 K respectively. Table 1 shows physical properties of solvent and water [21].

**Table 1 Physical properties of solvent and water**

| Physical Properties | Hydrocrarbon Solvent (ShellSoll D40) | Water |
|---|---|---|
| Specific density, [$kgm^{-3}$] | 785 | 998.2 |
| Molecular weight, [$gmol^{-1}$] | 146 | 18 |
| Specific enthalpy of evaporation, [$kJkg^{-1}$] | 306 | 2265 |
| Specific heat, [$Jkg^{-1}K^{-1}$] | 2090 | 4.182 |
| Critical temperature, [K] | 701.18 | - |
| Critical pressure, [atm] | 65.6 | - |

## 3. Theoretical consideration

In this section heat and mass transfer rates at different pressures were calculated in order to validate the numerical model. The thermal resistance of the insulating paper was not taken into account in the heat transfer calculations. Due to the water coming from the surface of the insulation paper into the solvent, the relative humidity decreases and the water that is insde the insulation paper diffuses to the surface. Therefore, the heat transfer on the surface is taken into account in the caldulations.

### 3.1. Calculation of mass diffusion coefficient

The mass diffusion coefficient which is calculated from kinetic theory is the proportionality factor D in Fick`s law, so it is directly proportional to temperature and inversely proportional to the pressure [22]. Equation 1, based on kinetic theory, applies to gases at low pressures.

$$\frac{PD_{ws}}{\left(P_{cr,w}P_{cr,s}\right)^{\frac{1}{8}}\left(T_{cr,w}T_{cr,s}\right)^{\frac{5}{12}}\left(\frac{1}{M_w}+\frac{1}{M_s}\right)^{\frac{1}{2}}} = a\left(\frac{T}{\left(T_{cr,s}T_{cr,w}\right)^{\frac{1}{2}}}\right)^{b} \quad (1)$$

**Table 2 Calculated mass diffusion coefficients for ShellSol D40 under different pressure**

| Pressure, [kPa] | 2.0 | 2.5 | 3.0 | 3.5 | 4.0 | 4.5 | 5.0 | 5.5 | 6.0 |
|---|---|---|---|---|---|---|---|---|---|
| $D_{ws}x10^{-4}$, [$m^2s^{-1}$] | 7.2 | 5.7 | 4.8 | 4.1 | 3.6 | 3.2 | 2.9 | 2.6 | 2.4 |

The constants *a* and *b* in eq. (1) were taken as $3.640x10^{-4}$ and 2.334 since ShellSol D40 is a polar gas. Using eq. (1), the mass diffusion coefficients for ShellSol D40 under different pressures were calculated and are shown in tab. 2. The coefficient of mass diffusion from air to water at the transformer surface is calculated by the following equation.

$$D_{aw} = \frac{9.25\cdot10^{-4}}{P_a}\cdot\frac{T^{2.5}}{T+245} \quad (2)$$

### 3.2. Calculation of mass diffusion coefficient

Heat and mass transfer can be expressed with similar dimensionless quantities. For example, heat transfer is expressed as a function of the Reynolds number (Re), Prandtl number (Pr), and Nusselt number (Nu), while the mass transfer in forced convection is expressed as a function of the Sherwood number (Sh), Reynolds number, and Schmidt number (Sc). Water vapor density over the insulation of the transformer is calculated by the following equation;

$$\rho_0 = \frac{P_{w,0}}{R_w T_0} \quad (3)$$

**Table 3 Water vapor density, solvent and Grashorf number under different pressure for heat and mass transfer**

| Pressure, [kPa] | Density, [$kgm^{-3}$] | | | Gr |
|---|---|---|---|---|
| | Solvent | Water | Average | |
| 2.0 | 0.096 | 0.031 | 0.063 | $9.17\cdot10^{11}$ |
| 4.0 | 0.191 | 0.031 | 0.111 | $1.29\cdot10^{12}$ |
| 6.0 | 0.287 | 0.031 | 0.159 | $1.44\cdot10^{12}$ |
| 6.5 | 0.310 | 0.031 | 0.111 | $1.15\cdot10^{12}$ |
| 8.0 | 0.382 | 0.031 | 0.206 | $1.52\cdot10^{12}$ |
| 10.0 | 0.478 | 0.031 | 0.254 | $1.57\cdot10^{12}$ |
| 12.0 | 0.573 | 0.031 | 0.302 | $1.61\cdot10^{12}$ |

The Grashof number (Gr) that is a dimensionless quantity used for natural convection is calculated using eq. (4) [3]. Water vapor density and Grashof number under different pressures for heat and mass transfer were shown in tab. 3.

$$Gr_m = g(\rho_s - \rho_w)\frac{d^3}{v^2\overline{\rho}} \tag{4}$$

Schmidt number that is the mass transfer equivalent of Prandtl number is the mass diffusivity rate of momentum diffusivity and is used to characterize fluid flows where there are simultaneous momentum and mass diffusion-convection processes [22].

$$Sc = \frac{v}{D_{ws}} \tag{5}$$

The Sherwood number that is a dimensional number used in mass transfer operation represents the ratio between convective mass transfer and the diffusive mass transport. The Nusselt number that is used for natural convection conditions is used in the calculation of mass transfer equations. Since the velocity in the drying chamber is almost zero. Instead of Gr and Pr numbers used in heat transfer equations Gr and Sc numbers which are used in mass transfer equations were used and thus the heat transfer equation was converted to mass transfer equation as shown in tab. 4.

**Table 4 Functional relation to the boundary layer analogies**

| | |
|---|---|
| Heat Transfer | $Nu = A\left(Gr^b\ \mathrm{Pr}^n\right) = hd/k = 0.59\cdot(Gr\cdot\mathrm{Pr})^{0.25}$ |
| Mass Transfer | $Sh = A\left(Gr_m^b Sc^n\right) = h_m d/D_{ws} = 0.59\cdot(Gr\cdot Sc)^{0.25}$ |

Moisture and heat transfer rates were calculated with the eq. (6) and (7), respectively. Table 5 shows that the mass and heat transfer calculations under different pressures, while the average and maximum results of mass and heat transfer calculations were shown in tab. 6. The condensation of the solvent vapor was calculated using eq. (8).

**Table 5 Heat and mass transfer calculation under different pressures**

| | Mass Transfer | | | | | Heat Transfer | | |
|---|---|---|---|---|---|---|---|---|
| Pressure [kPa] | *Sc* | *Sh* | $h_m$ [ms$^{-1}$] | $\dot{m}_v$ [kgs$^{-1}$] | $\dot{Q}_{evo}$ [kW] | *Pr* | *h* [Wm$^{-2}$K$^{-1}$] | $\dot{Q}_{heat}$ [kW] |
| 2.0 | $2.40\cdot10^{-2}$ | 227.24 | 0.059 | 0.095 | 229.95 | 0.088 | 5.19 | 28.25 |
| 4.0 | $4.80\cdot10^{-2}$ | 294.47 | 0.038 | 0.061 | 148.99 | 0.176 | 6.73 | 36.61 |
| 6.0 | $7.20\cdot10^{-2}$ | 334.92 | 0.029 | 0.046 | 112.97 | 0.264 | 7.65 | 41.64 |
| 6.5 | $4.80\cdot10^{-2}$ | 277.77 | 0.045 | 0.071 | 134.27 | 0.308 | 7.74 | 42.15 |
| 8.0 | $9.59\cdot10^{-2}$ | 364.81 | 0.024 | 0.038 | 92.29 | 0.352 | 8.33 | 45.35 |
| 10.0 | $1.20\cdot10^{-1}$ | 388.88 | 0.020 | 0.032 | 78.70 | 0.440 | 8.88 | 48.35 |
| 12.0 | $1.44\cdot10^{-1}$ | 409.21 | 0.018 | 0.028 | 69.02 | 0.528 | 9.34 | 50.88 |

**Table 6 Heat and mass transfer results for average and maximum rate**

| Mass Transfer Results | | Heat Transfer Results | |
|---|---|---|---|
| $\overline{Gr}$ | | $1.15 \cdot 10^{12}$ | |
| $\overline{D}_{ws}$ | $2.39 \cdot 10^{-4}$ | Nu | 213 |
| $\overline{Sc}$ | $4.80 \cdot 10^{-2}$ | $h_{heat}$ | 3.51 [$Wm^{-2}K^{-1}$] |
| $\overline{Sh}$ | 277.77 | $\dot{Q}_{heat}$ | 30 [kW] |
| $\overline{h}_m$ | 0.045 [$ms^{-1}$] | $\dot{m}_{cs}$ | 0.511 [$kgs^{-1}$] |
| $\dot{m}_{v,avg}$ | 0.071 [$kgs^{-1}$] | | |
| $\dot{Q}_{evo,max}$ | 230 [kW] | | |

$$\dot{m}_w = \overline{h}_m \cdot A \cdot \left(\rho_{w,0} - \rho_{w,\infty}\right) \tag{6}$$

$$\dot{Q}_{evo} = \dot{m}_w \cdot h_{ws} \tag{7}$$

$$\dot{Q}_{total} = \dot{m}_{cs} \cdot c_{p,s} \cdot \left(T_{in} - T_{cs}\right) + \dot{m}_{cs} \cdot h_{fg,s} \tag{8}$$

## 4. Numerical study

### 4.1. CFD simulations

A 3D model for the VPD process was developed by using ANSYS/Fluent software. The computational domain was created using Ansys/Design Modeler for active part which consists of laminated core, windings and insulation materials of 200 MVA power transformer. It is necessary to simplify the model in order to create a solution network in compex CFD analysis like this study to reduce the computational CPU time and usage. The transformer is monophase transformer with 200 MVA power, so it has two columnar cores. Vapor phase drying chamber and computational domain of it were shown in fig. 1(a) and (b), respectively.

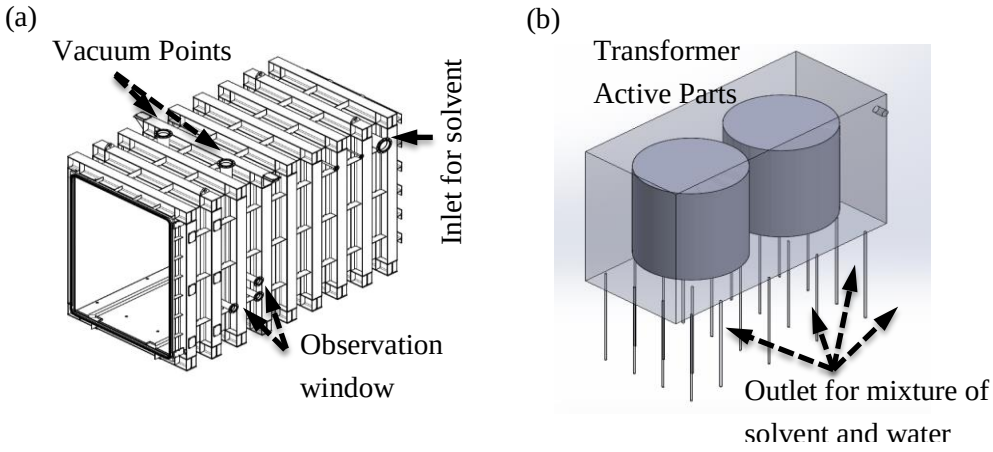


**Figure 1 (a) Vapor phase drying chamber (b) Computational domain of vapor phase drying chamber**

Continuity, momentum, turbulence, and energy equations were solved for the solvent. The realizable k-epsilon model that shows a good agreement with empirical calculation data was applied in the model in order to solve the turbulence. The turbulence model uses two equations in the k-epsilon method, expressed in Eulerian coordinates. Turbulent intensity and length scale method was used for the turbulent specification method.

### 4.2. Grid generation

Sufficient grid refinement in the computational domain is necessary to capture the computational stability and reliability of the results. It was created a tetrahedral mesh for the computational domain. Additionally, sweep mesh was used on the surface of insulation paper.

The meshes were refined near the wall of insulation paper, where more pressure gradient is expected. The mesh structure of the VPD chamber can be seen in fig. 2. The skewness is an important parameter to understand the grid structure quality. Mesh structure's skewness value is given 0.85, which is quite acceptable in literature.

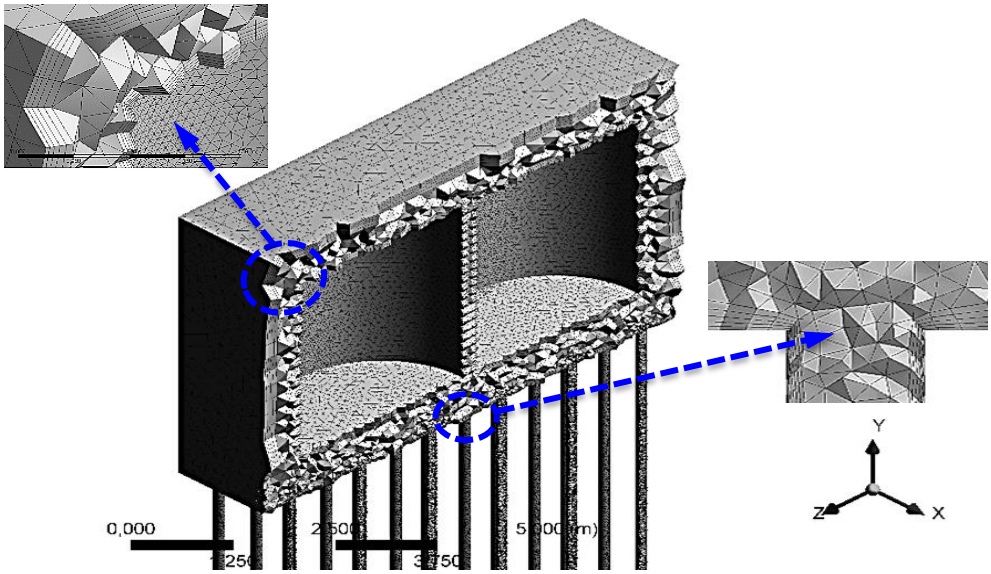


**Figure 2 Mesh structure of the computational domain**

### 4.3. Boundary conditions

The velocity inlet and the pressure outlet boundary condition were applied to the solvent and water inlet and solvent vapor mixture outlet, respectively. The energy withdrawn from the solvent vapor due to the condensing water is equal to be released from the surface of the drying chamber. Therefore, the wall boundary assumes to be at a fixed temperature, so standard wall function was applied to each wall boundaries.

In the heat transfer mechanism in the drying process, the condensation of solvent vapor was taken into consideration in both emprirical and CFD analysis. In the CFD analysis, a special User Defined Function (UDF) code was used to obtain the solvent vapor condensing event on the surface of insulating paper. When the defined condensation temperature was reached for each finite volume, a

UDF code was used to reduce the enthalpy of the solvent at constant temperature up to the condensation load. But there is no physical phase change in the numerical model. Thus, the solution is simplified. Heating was applied to two different locations, wall and inlet boundary. The constitutive equations were solved by using a pressure-based solution algorithm as transient. CFD analysis was performed at 168 hours using a 16-core workstation with 32 GB DDR4 RAM.

### 4.4. Validation and mesh independence

The numerical model was verified by comparing the CFD analysis results with the theoretical calculation data. Theoretical and computational errors range from 5.45 to 16.24% for low pressures (<5kPa) and from 2.25 to 3.43% for high pressures (over the 5 kPa). Figure 3 shows the theoretical and computational results of heat transfer rate over the insulation paper depending on the pressure. The average deviation between CFD results and theoretical calculations is 2.94% for transformer's heat transfer rate larger than 40 kW. The designed transformer's heat transfer rate corresponds to approximately 48 kW. Thus, the numerical results demonstrated a good accordance with the theoretical data.

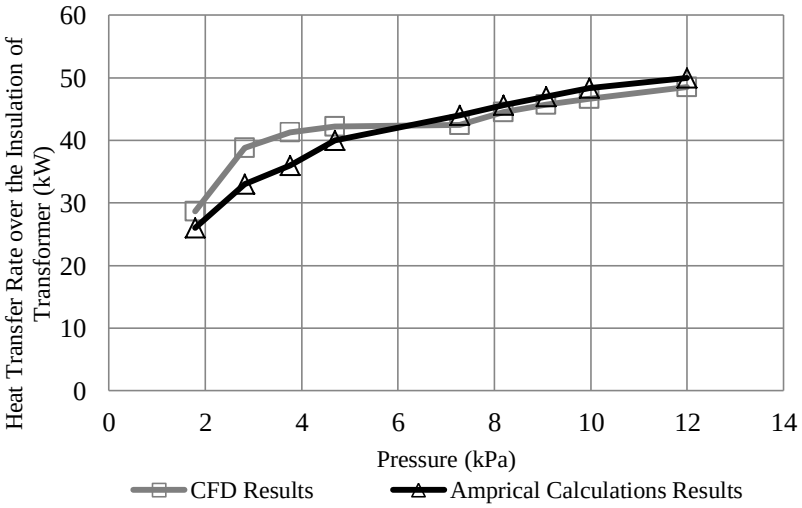


**Figure 3 Comparisons of the CFD results with theoretical calculation**

An independent mesh study was conducted, where the density of the nodes increased till the solution was no longer change with additional mesh refinement. For this purpose, the change in heat transfer rate through the insulation paper was followed depend on the increase in mesh count, and optimum grid density was determined. The numerical study was conducted with 10, 15, and 20 million volume element. Maximum deviation in heat transfer rate was %2.3. Thus, it was decided that 15 million volume elements were enough for the computational domain.

## 5. Results and discussions

CFD results were examined on different stages namely, the first heating phase, first vacuum phase, second heating phase and fine vacuum phase. The average pressure in the chamber and the temperature distribution over the insulation paper in each phase range were shown in fig. 4. The temperature reduces in the vacuum phase and increases in the heating phase. The temperature in the chamber varies depending on the pressure, so the system pressure can be adjusted to improve the yield in each phase.

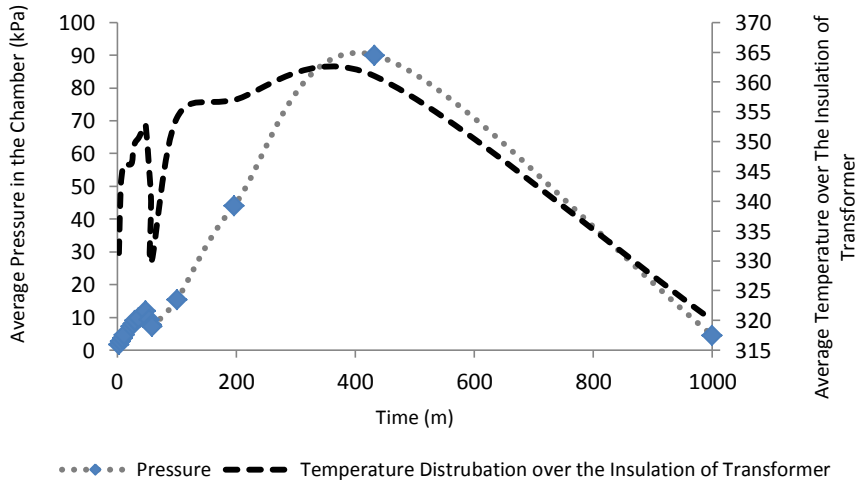


**Figure 4 Change of the temperature and average pressure in the chamber versus time**

### 5.1. First heating phase

The main purpose in this study is that the temperature distribution on the winding surfaces during the drying process is below 353 K. Therefore, the temperature distributions in the chamber ware not studied.

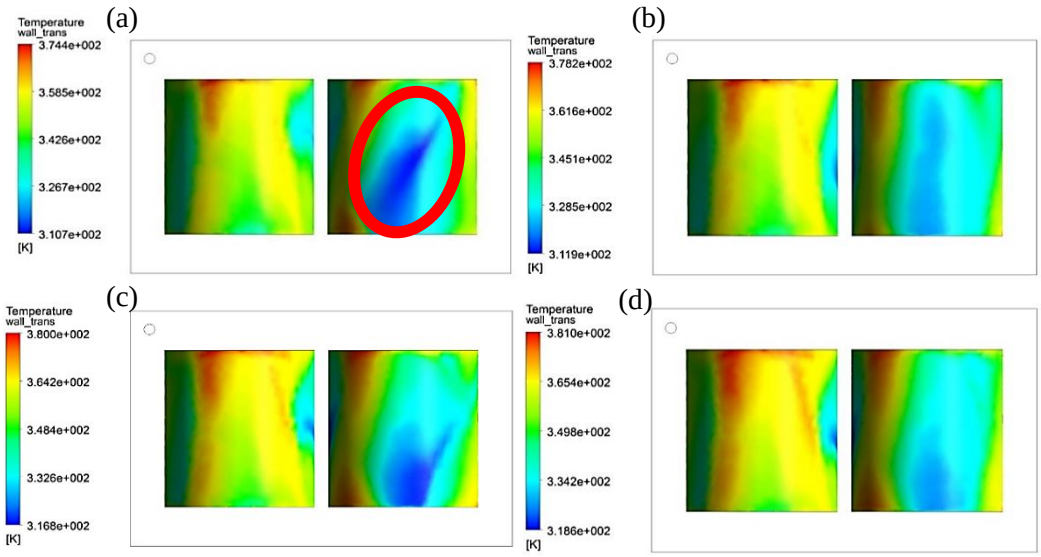


**Figure 5 Temperature distribution under different pressure (a) 3kPa, (b) 6 kPa, (c) 9 kPa and (d) 12kPa**

In this stage, the average temperature of surface of insulation paper reaches 353 K. The solvent enters into the chamber at 403 K from the inlet. Figure 5 shows that the temperature distribution under different pressure. The temperature scale is between 310.7 K and 374.4 K. The field pointed out in fig 5(a) was the lowest temperature area. The average temperature (353 K) was achieved at 12 kPa pressure and a satisfactory temperature distribution was also obtained at this pressure condition can be seen in fig. 5(d)

### 5.2. First vacuum phase

The chamber pressure at the beginning of the first vacuum phase was 12 kPa. Most of the solvent was drained out till the chamber pressure decrease to 7 kPa. Because of the low pressure, the internal gas that was formed in tiny intermediate parts and layers of the object could be discharged. Thus, solvent vapor can be entering these spaces and the heat exchange is facilitated. Temperature distribution at the end of the first vacuum phase in which the pressure was around 7 kPa, shown in fig. 6. Maximum temperature was reduced to 335 K.

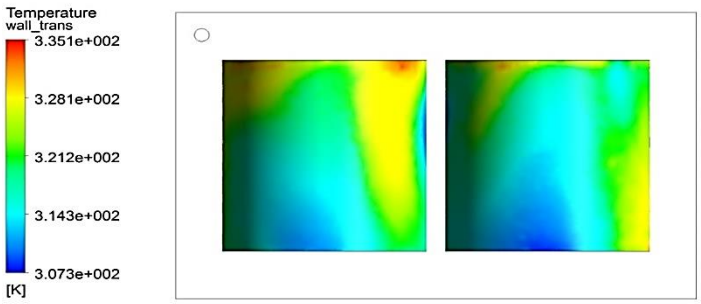


**Figure 6 Temperature distribution at 7 kPa**

### 5.3. Second heating phase

In this stage, the solvent sent to the chamber until the average temperature on the insulation paper reaches to 363 K. The pressure reaches 90 kPa when the average temperature is 363 K. The temperature distribution was shown in fig 7 at 90 kPa pressure and 363 K average temperature conditions. The maximum temperature obtained on the insulation was 384.3 K, which was still below the critical temperature of 403 K. Total heat transfer is 40 kW of which 17 kW is caused by mass transfer, and 23 kW is due to temperature difference.

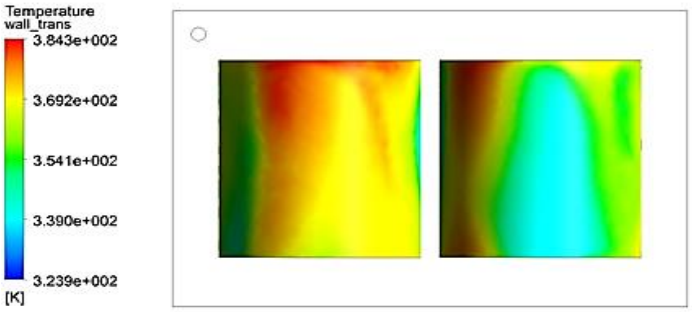


**Figure 7 Temperature distribution at level to 90 kPa and 363 K.**

### 5.4. Fine vacuum phase

The solvent is drained out from the chamber until the chamber pressure reduces to 4.5 kPa in the fine vacuum phase that is the final phase. Here, moisture is evacuated from the chamber. The temperature distribution of this phase was shown in fig 8. A homogeneous temperature distribution on the insulation paper has been achieved and moisture level over the insulation paper was decreased below 2%.

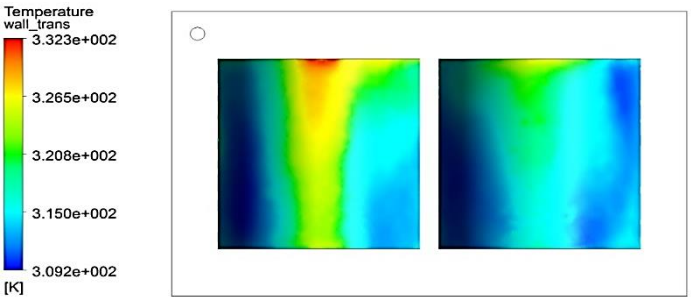


**Figure 8 Temperature distribution at 4.5 kPa**

Drying chamber was optimized by using ANSYS/Response Surface Optimization software that explores the relationship between design variables and one or multiple response variables. The nonlinear programing by quadratic lagrangian (NLPQL) method that supports a single objective, multiple constraints and is limited to continuous parameters is used for optimization method. The design variables were inlet and outlet position, and dimensions of the drying chamber, while response variable was mass transfer rate. After defining the minimum and maximum values that the design variables could take, the mass transfer rate was maximized to shorten the cycle time of the drying process. At the end of the computer-assisted optimization process, the most appropriate inlet and exit positions and drying chamber design were determined. The drying chamber volume was reduced by 8% and the dimensions were arranged to be 3.5m in wide, 3.5m in height and 7m in deep. The drying process cycle time is reduced to 12 hours with the new design. Considering that the drying process duration for VPD and the conventional vacuum drying method is 14 hours and 18 hours respectively [13], it is clear that the drying cycle time with the new design has been reduced considerably.

The mass transfer rate is 0.004 m/s when the air is used in the drying process, while it is 0.045 m/s when the solvent is used. Due to the windings of the transformer structure, the sufficient amount of solvent cannot be sent to the channels, and as a result of this, an efficient drying process does not occur in the drying chamber. Consequently, the large difference in mass transfer rate on the surface does not shorten the duration of the drying process as expected. But it is clear that the solvent usage was shortened the cycle time. The drying process that takes almost 15 hours was decreased to 3 hours with the solvent as a heat carrier instead of air for one cycle.

## 6. Conclusions

In this paper a theoretical and numerical study was conducted to improve the drying chamber design. The effect of the solvent in the transformer drying process was investigated and VPD process was optimized using CFD method. Owing to the new drying chamber design the drying process time was decreased. The main conclusions are summarized as follows.

- In the first heating phase, an average temperature of 353 K was obtained on the insulation of the transformer at 12 kPa. The temperature on the insulation paper had risen to a maximum of 381 K, which was below the transformer's surface safety temperature of 403 K. In addition, under these conditions, a satisfactory temperature distribution on the insulation paper was achieved. In the second heating phase, a maximum temperature of 384.3 K on the insulation paper was reached, which was still below the critical temperature of 403 K.
- The new design can be used during the drying process of power transformers, since the moisture level over the insulation paper is reduced below 2%, so the transformer service life was extended.
- Due to the new design of the drying chamber, the drying process time was decreased almost 14.3%. Thus, the operation cost of the drying process was decreased.
- When the solvent is used instead of air as the heat carrier, the drying cycle time was reduced almost 20%.

**Acknowledgment**

The authors would like to thank the Scientific and Techological Research Council of Turkey (TUBITAK) for their financial support. This project was partially funded by TUBITAK TEYDEB 1501 Program with the project no: 3130152.

**Nomenclature**

| | | | | | |
|---|---|---|---|---|---|
| A | = | Area, [$m^2$] | R | = | Gas constant, [$Jmol^{-1}K^{-1}$] |
| D | = | Mass diffusion coefficient, [$m^2s^{-1}$] | Re | = | Reynolds number, $(=Ud/v)$, [-] |
| d | = | Diameter of windings, [$m^2$] | Sh | = | Sherwood number, $(=h_m d/D)$, [-] |
| g | = | Gravity, [$ms^{-2}$] | Sc | = | Schmidt number, $(=v/D)$, [-] |
| Gr | = | Grashof number, [-] | T | = | Temperature, [K] |
| h | = | Heat transfer coefficient, [$Wm^{-2}K^{-1}$] | Q | = | Heat transfer rate, [W] |
| $h_{fg}$ | = | Evaporation enthalpy, $kjkg^{-1}$ | *Greek symbols* | | |
| $h_m$ | = | Mass velocity, [$ms^{-1}$] | ρ | = | Density, [$kgm^{-3}$] |
| k | = | Thermal conductivity coef., [$Wm^{-1}K^{-1}$] | ν | = | Kinematic viscosity, [$m^2s^{-1}$] |
| M | = | Molecular weights of gas species [-] | *Subscripts* | | |
| Nu | = | Nusselt number, $(=hd/k)$, [-] | a | = | Air |
| P | = | Pressure, [Pa] | aw | = | Air to water vapour |
| Pr | = | Prandtl number, $(=\mu c_p/k)$, [-] | cs | = | Condensing solvent |
| evo | = | Evoparation | w | = | Water vapour |
| heat | = | Heat transfer | ws | = | Water vapour to solvent |
| cr | = | Critical value | o | = | Surface |
| m | = | Mass transfer | ∞ | = | Ambient |
| s | = | Solvent | | | |

**References**

[1] Arshad, M., Islam, S., Significance of cellulose power transformer condition assessment, *IEEE Transactions on Dielectrics and Elecrtical Insulation, 18* (2011), 5, pp. 1591-1598.

[2] Kudra, T., Mujumdar, A., *Advanced Drying Technologies,* Taylor & Francis Group, NewYork, ,USA, 2009.

[3] Bangar, A. et al., Comparative analysis of moisture removing processes from transformer which are used to increase its efficiency, *Global Journal of Research in Engineering , 12* (2012), 5, pp. 7-12.
[4] Orikasa, T. et al., Impacts of hot air and vacuum drying on the quality attributes of kiwifruit slices, *Journal of Food engineering , 125* (2014), pp. 51-58.
[5] Padmanabhan, S. et al., Synthesis of silica cryogel-glass fiber blanket by vacuum drying, *Ceramics International , 42* (2016), 6, pp. 7216-7222.
[6] Patil, V. et al., Optimizationof the spray-drying process for developing guava powder using response surface methodology, *Powder Technology , 253* (2014), pp. 230-236.
[7] Atalar, I., Dervisoglu, M., Optimization of spray drying process parameters for kefir powder using respons surface methodology, *LWT - Food Science and Technology , 60* (2015), 2, pp. 751-757.
[8] Erbay, Z. et al., Optimization of spray drying process in cheese powder production, *Food and Bioproducts Processing, 93* (2015), pp. 156-165.
[9] Cho, J. et al., Large-scale production of fine-sized Zn2SiO4:Mn phosphor microspheres eith a dense structure and good photoluminescence properties by a spray-drying process, *Royal Society of Chemistry , 4* (2014), pp. 43606-43611.
[10] Son, M. et al., Study of Co3O4 mesoporous nanosheets propared by a simple spray-drying mprecess and their electrochemical properties as anode material for lithium secondary batteries, *Elecrochimica Acta , 116* (2014), pp. 44-50.
[11] Jeon, K. et al., Elecrochemical properties of MnS-C and MnO-C composite powders prepared via spray drying process, *Journal of Powder Sources , 295* (2015), pp. 9-15.
[12] Park, G. et al., Large-scale production of MoO3-reduced graphene oxide powders with superior lithium storage properties by spray-drying process, *Electrochimica Acta , 173* (2015), pp. 581-587.
[13] Swassisevi, T. et al., Optimizaion of a drying process using infrared-vacuum drying of Cavendish banana slices, *Songklanakarin Journal of Science and Technology, SJST, 29* (2007), 3, pp. 809-816.
[14] Giri, S.K., Prasad, S. Optimization of microwave-vacuum drying of button mushrooms using response surface methodology, *Drying Technology, 25* (2007), 5, pp. 901-911.
[15] Han, Q.H. et al., Optimization of process parameters for microwave vacuum drying of apple slices using response surface method, *Drying Technology, 28* (2010), 4, pp. 523-532.
[16] Sturm, B. et al., Optimizing the drying parameters for hot-air-dried apples, *Drying Technology, 30* (2012), 14, pp. 1570-1582.
[17] Pu, Y.Y., & Sun, D.W., Combined hot-air and microwave-vacuum drying for improving uniformity of mango slices based on hyperspectral imaging visualization of moisture content distribution, *Biosystems Engineering, 156* (2017), pp. 108-119.
[18] Silva, P.I. et al., Parameter optimization for spray-drying microencapsulation of jaboticaba (myrciaria jaboticaba) peel extracts using simultaneous analysis of responses, *Journal of Food Engineering, 117* (2013), pp. 538-544.
[19] Kumar, D. et al., Optimization of microwave-assisted hot air drying conditions of okra using response surface methodology, *Journal of Food Science and Technology, 51* (2014), 2, pp. 221-232.
[20] Siddiqui, M. et al., Vapor Phase Drying for Moisture Removal from Transformer Coil Insulation, *Intrnational Journal of Scientific & Engineering Research, IJSER , 8* (2017), 4, pp. 20-24.

[21] ***, Shell, https://www.shell.com (accessed 28 May 2018).

[22] Incropera, F. et al., *Fundementals of heat and mass transfer* (6th *Edition ed.)*, John Wiley & Sons, Danvers, USA, 2007.